Journal of Alloys and Compounds 557 (2013) 172–178

Contents lists available at SciVerse ScienceDirect

Journal of Alloys and Compounds

journal homepage: www.elsevier.com/locate/jalcom

Structural and magnetic investigations on metastable Ag–Fe nanophase alloy

Kalavathy Santhi [a,d], E. Thirumal [a], S.N. Karthick [b], Hee-Je Kim [b], V. Narayanan [c], A. Stephen [a,*]

[a] Material Science Centre, Department of Nuclear Physics, University of Madras, Guindy Campus, Chennai 600 025, India
[b] School of Electrical Engineering, Pusan National University, Jangjeon, Geumjeong, Busan 609-735, Republic of Korea
[c] Department of Inorganic Chemistry, University of Madras, Guindy Campus, Chennai 600 025, India
[d] Department of Physics, Women's Christian College, Chennai 600 006, India

ARTICLE INFO

Article history:
Received 13 September 2012
Received in revised form 7 November 2012
Accepted 30 December 2012
Available online 5 January 2013

Keywords:
Metals and alloys
Chemical synthesis
Magnetic measurements
Thermal analysis
Nanostructured materials

ABSTRACT

Nanocrystalline Ag–Fe alloy samples of various compositions were synthesized by chemical reduction method using sodium borohydride as the reducing agent. The structure analysis of the as prepared and the annealed samples were carried out. The fcc structure of the as prepared samples was stable up to 400 °C. As bulk Ag and Fe are immiscible metals, nanophase alloy formation of these two metals was studied from the broad exothermic peak observed and the enthalpy changes were calculated from the differential scanning calorimetric analysis. The presence of Ag and Fe in their metallic form was verified by performing X-ray photoelectron microscopy studies. The microstructure of these samples reveals that the particles are nanosized. The results of the magnetic characterization of the as synthesized and annealed $Ag_{50}Fe_{50}$ sample and the conclusions drawn there from are in correlation with the metastable nature of the samples up to 400 °C and the phase changes in the sample annealed at 500 °C.

1. Introduction

In granular alloys consisting of single domain magnetic particles in a nonmagnetic matrix, phenomena such as giant magnetoresistance and interparticle magnetic interactions through nonmagnetic spacers are prominent. In the case of immiscible alloy systems such as Ag–Fe, where the heat of mixing is positive, the solid solubility is almost negligible under equilibrium conditions [1]. In general even when the elements forming certain alloys have bulk immiscibility as per their phase diagrams, studies reveal that alloying is possible at the nano-level [2]. There are experimental evidences to show nanomaterial alloy formation of several immiscible systems which have positive heat of mixing. Therefore when these nano-phase alloys are obtained, they have sharp interfaces between the magnetic and the nonmagnetic components which play a significant role in changing their magnetic coupling effects. The at.% of the magnetic component not only influences the magnetic moment, but also the magnetic interactions by altering the proximity of the magnetic atoms and hence gives rise to materials with unique magnetic properties. In addition to their magnetic properties their stability is also improved by the encapsulating nonmagnetic noble metal atoms. Hence synthesis and study of such systems have gained importance in recent years. But only certain methods are helpful in producing these alloy nanomaterials. A few studies on Ag–Fe alloy systems synthesized by electrodeposition, vapor quenching, sol–gel method, sputtering, molecular beam epitoxy, etc., have been reported in literature [3–7]. Ma et al. have reported that Ag and Fe did not show any miscibility when subjected to mechanical milling, though alloy formation of immiscible Cu–Fe was possible by the same method [8]. These alloy nanomaterials are normally in metastable state. In order to understand the application potential of these magnetic materials, their thermal stability needs to be analyzed. Hence it is appropriate to study the effects of annealing on the structure and the magnetic behavior of the alloy samples as done in a few previous studies on Ag–Fe samples prepared by sputtering and by sol–gel method [9,10] and on mechanically alloyed Fe–Cu solid solution which is of the same kind [11]. Materials such as Co–Ag, Fe–Ag, Co–Cu, Fe–Cu, Co–Pt, Fe–Pt, etc., with ferromagnetic and nonmagnetic interfaces are largely used in sensors, spin valves and high density recording devices, etc., [12–14].

In this work nanocrystalline Ag–Fe alloy was synthesized by borohydride reduction method and its stability was studied by annealing the as prepared sample at various temperatures in vacuum. Borohydride reduction method is a widely used method for synthesis of single metal nanoparticles [15,16]. It is found to be an effective method even for preparation of alloy nanomaterials.

2. Experimental details

Ag–Fe nanomaterial was synthesized in different compositions viz. Ag_xFe_{100-x} (x = 100, 90, 75, 50 and 25) by simultaneously reducing an aqueous solution of $AgNO_3$ and $Fe(NO_3)_3$. The metal salts were taken in ratios 90:10, 75:25, 50:50 and 25:75 along with sodium citrate as the stabilizing agent to form the precursor. The ratio of $NaBH_4$ and the total metal concentration was made as 15:1 in order to ensure complete reduction. The details of the synthesis method have been reported elsewhere [17].

* Corresponding author. Tel.: +91 44 22202802; fax: +91 44 2235 3309.
E-mail address: stephen_arum@hotmail.com (A. Stephen).

0925-8388/$ - see front matter © 2013 Elsevier B.V. All rights reserved.
http://dx.doi.org/10.1016/j.jallcom.2012.12.161

The composition of the metals in the alloy samples were determined using Perkin Elmer Optima 5300 DV Inductively coupled plasma optical emission spectroscopy (ICP-OES). X-ray photoelectron spectroscopy (XPS) measurements were made with Omicron ESCA Probe spectrometer with monochromatized Al Kα X-rays ($h\nu$ = 1486.6 eV) to confirm the electronic states of the constituent metals. The structure of the material was determined using the X-ray diffraction patterns obtained at room temperature using X-ray diffractometer in Bragg–Brentano geometry (3003 TT) with Cu $K\alpha_1$ (λ = 0.15405 nm) radiation. The Differential Scanning Calorimetry (DSC) studies were carried out on NETZSCH STA 449F3 in nitrogen atmosphere. Field emission scanning electron microscopy (FESEM) equipped with energy dispersive X-ray spectrometer (EDX) (SU6600, Hitachi) was used to analyze the morphology and a high resolution transmission electron microscopy (JEOL model JEM 2011) was employed to study the microstructure of the samples. The magnetic behavior was recorded using a vibrating sample magnetometer (VSM, EG&G PARC, Model 4500) with a maximum applied field of 600 kA/m at room temperature. Mössbauer spectra of the as prepared and the annealed samples were recorded at room temperature using Nucleonix Mössbauer spectrometer in transmission geometry. The spectrometer was calibrated before each sample run using the spectrum of pure natural Fe foil.

3. Results and discussion

3.1. Structure analysis

The XRD patterns of the as prepared Ag–Fe materials obtained from precursors of different compositions are shown in Fig. 1. These patterns exhibit clear fcc structure peaks (111), (200), (220) and (311) resembling that of silver (JCPDS card no. 893722) for all the as synthesized samples. The Fe rich $Ag_{25}Fe_{75}$ sample also has the same fcc structure and it shows some amorphousity. Though the peak positions of bcc Fe (110), (200) and (211), (JCPDS card no. 851410) almost overlap with the fcc peak positions of the alloy [18], the intensities of these peaks are found to be matching with the relative intensities of the fcc Ag peaks with the (111) peak having the maximum intensity. This is largely due to the formation of Ag–Fe alloy with atomic level mixing of Fe in the Ag lattices. However, there is a possibility of a small fraction of ultra fine Fe nanoparticles within the superparamagnetic limit being embedded in the fcc matrix in the as prepared form without any contribution to bcc phase. These iron-rich islands which are too small to be considered as a precipitated phase, may practically fit into the lattice in which they are incorporated. Even in a few other works on Ag–Fe, only the fcc structure peaks have been observed in the as synthesized form which then undergoes phase transformation on heat treatment. In some cases these peaks have been indexed as Ag–Fe peaks [3,19–21]. In a few cases prominent bcc Fe peaks with higher intensity are also observed along with the fcc peaks, for Fe contents above 40 at.% [22]. Similar fcc Ag peaks in the case of Ag–Ni particles prepared by gas condensation method [23] and in the case of Ag–Co alloy synthesized by different methods [24,25] have been reported in literature. There is no detectable amount of iron oxide at low concentrations. But at higher concentrations of Fe, a small hump is speculated at 35.6° due to surface oxidation. The average crystallite sizes of the as synthesized pure Ag, $Ag_{90}Fe_{10}$, $Ag_{75}Fe_{25}$, $Ag_{50}Fe_{50}$ and $Ag_{25}Fe_{75}$ samples were calculated using Scherrer formula from the most prominent peak (111) as 38, 29, 28, 22 and 31 nm respectively. The particle sizes show a decrease with increase in Fe content, but an increase for the sample with 75% Fe. A similar trend in grain size changes in Ag rich and Fe rich Ag–Fe alloy samples grown by pulsed laser deposition has been reported by Störmer and Krebs [26].

The XRD patterns of the as prepared sample $Ag_{50}Fe_{50}$ as well as that annealed at 300 °C, 400 °C and 500 °C are shown in Fig. 2. It can be seen that the samples annealed at 300 °C and at 400 °C for 1 h have the same fcc structure as the as-prepared sample without any phase separation peaks or variation in peak intensities. There is also no significant growth in the sizes of the particles. This implies that the fcc phase of the alloy sample is stable up to 400 °C. A small peak of Iron oxide is seen at 2θ values of 35.6° and 62.9° corresponding to (311) and (440) peaks of γ-Fe_2O_3 primitive cube after heat treatment (JCPDS card no. 895892). In the case of the sample annealed at 500 °C, the intensity of the peaks corresponding to bcc Fe (110) and Fe (200) increase with a decrease in the intensity of Ag (111) peak. Hence, above 400 °C, the fcc alloy phase further enriches with Fe atoms and when the Fe content in the crystallites increase beyond a certain limit they transform into bcc Fe phase. Similar phase changes have been observed in the case of heat treated Fe–Cu solid solution [11]. Another possibility is that the tiny Fe nanoparticles which are present in the fcc Ag matrix could have grown beyond the critical size and separated out when heated above 400 °C. Due to these causes, the sample annealed at 500 °C exhibits an increase in intensity of peaks which correspond to bcc Fe (110) and Fe (200). The XRD results of the heat treated samples indicate that the alloy samples are metastable which decompose beyond 400 °C. The same result is reflected in the magnetic measurements and the thermodynamical analysis.

3.2. Composition analysis

The metal contents in the alloy samples were determined by the well established ICP-OES analysis. The samples were completely

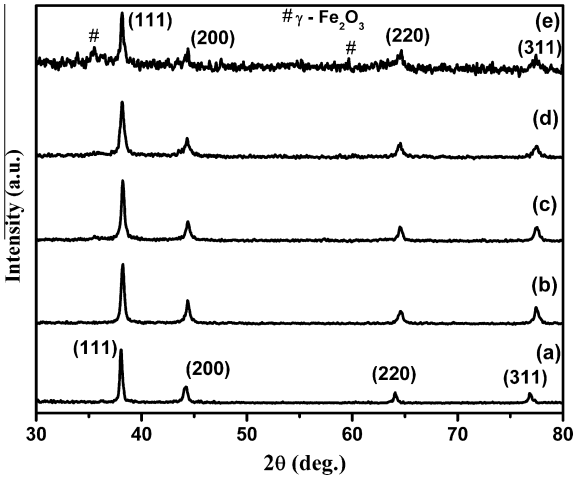

Fig. 1. XRD patterns of as prepared (a) pure Ag, (b) $Ag_{90}Fe_{10}$, (c) $Ag_{75}Fe_{25}$, (d) $Ag_{50}Fe_{50}$ and (e) $Ag_{25}Fe_{75}$ samples exhibiting fcc structure.

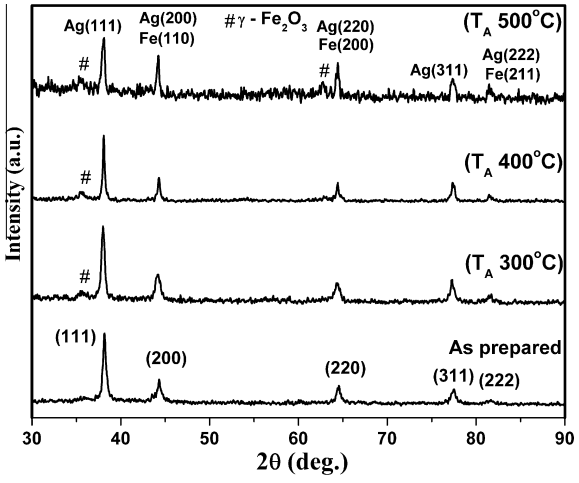

Fig. 2. XRD patterns of as synthesized and annealed $Ag_{50}Fe_{50}$ sample in vacuum at 300 °C, 400 °C and 500 °C. The sample has fcc structure up to 400 °C and precipitation of Fe into bcc structure is speculated at 500 °C.

dissolved in a small quantity of a mixture of nitric and sulfuric acid and used for analysis. The Ag and Fe metal ratios in the samples prepared from precursors containing $AgNO_3$ and $Fe(NO_3)_3$ in different ratios are shown in Table 1. The data given in the table clearly shows that both Ag and Fe are present in compositions close to their salt ratios in precursors. Hence Ag–Fe alloy of any desired composition can be easily synthesized by taking suitable salt ratios.

3.3. X-ray photoelectron spectroscopy analysis

XPS analysis was done for the as prepared $Ag_{50}Fe_{50}$ alloy sample to confirm the presence of the constituent metals in their metallic form and to determine the different charge states of the components present and to study the chemical composition of the sample. A few studies reveal that XPS measurement is used as a tool to distinguish between metallic and different oxidation states, as it helps to find the charge states of the metal species in alloy and bimetallic systems [27,28]. Fig. 3a presents the survey spectrum of the sample confirming the presence of the 3d and 3p states of Ag and the 2p state of Fe along with the oxygen peak. Fig. 3b shows the two components of Ag 3d spectrum. The Ag $3d_{5/2}$ and Ag $3d_{3/2}$ peaks occurring at the binding energies of 368.3 and 374.3 eV with a difference of 6.0 eV can be assigned to metallic Ag [29].

The 2p Fe region shown in Fig. 3c as a function of the binding energy of the emitted electrons for the sample has two peaks accompanied by various shoulders. The two main peaks at 707.1 eV and 720.3 eV with an energy spacing of 13.2 eV are due to $2p_{3/2}$ and $2p_{1/2}$ emission of metallic Fe [30,31]. The two resolved peaks seen at 711.1 and 724.7 eV can be attributed to the Fe $2p_{3/2}$ and Fe $2p_{1/2}$ states of Fe^{3+} ions. The fine structure splitting of these two components 13.6 eV is indicative of Fe^{3+} ions that originate from the formation of γ-Fe_2O_3 on the surface of the nanoparticles due to oxidation [32]. This result is in accordance with the XRD analysis which exhibits the presence of γ-Fe_2O_3 in the heat treated samples. The two shoulders on the higher energy side at 714.5 eV and 728.5 eV represent the satellite peaks associated with Fe 2p. These satellite peaks also support bonding of oxygen with Fe possibly to form iron oxide on the surface. The peak observed at 531.2 eV as shown in Fig. 3d can be assigned to the oxygen bonded with Fe [33].

3.4. DSC analysis

The DSC plots of the samples $Ag_{90}Fe_{10}$, $Ag_{75}Fe_{25}$ and $Ag_{50}Fe_{50}$ were obtained to make the thermodynamical assessment of the processes involved in heat treating the samples and are shown in Fig. 4 a–c. The heating rate was maintained at 10 °C per minute and the samples were kept in N_2 flow of 10 cc/min to prevent oxidation during analysis. The DSC traces show a very broad exothermic peak from 150 °C to 750 °C. Similar broad hump has been observed around 300 °C by Kataoka et al, for $Fe_{0.87}Ag_{0.13}$ sample with the heat of mixing calculated as 10 kJ/mol [34]. Though not many reports are available on the thermodynamical studies of Ag–Fe system, the change in enthalpy calculated based on the DSC measurements can be compared with similar immiscible systems such as Ag–Ni and Fe–Cu reported in literature [17,35,36]. The broad exothermic peak represents the different processes taking place in this temperature range and hence fitted into three Gaussian peaks (see supplementary data Fig. S1a–c). Similar thermal behavior has been reported in the case of some nanocrystalline alloys [37,38]. These processes include the possible atomic disorder–order transition in the fcc structured nanocrystalline samples, growth in size of the alloy particles and precipitation of Fe atoms above 400 °C. Deconvolution of the broad exothermic peak into its components for calculating the enthalpy changes during each process has been reported by Huang [39]. The heats of mixing integrated from the first constituent peak are 22.7, 26.9 and 29.2 kJ/mol for the samples with 3.4, 17.7 and 46.3 at.% of Fe respectively. These enthalpy values are of the same order and show a gradual increase with increase in Fe content up to 50–55% and then a decrease, as reported in the case of Fe–Cu and Ag–Ni [35]. This is followed by the second deconvoluted peak which denotes the process involving enhancement of long range ordering and growth in size of the particles. Since these are systems with a large miscibility gap, very long range ordering is not favoured in their as prepared form. The third peak above 400 °C represents crystallization of Fe atoms due to precipitation. Hence the next exothermic profile above 400 °C is attributed to the growth of the bcc Fe phase which is in correlation with the XRD results of the samples annealed at 300, 400 and 500 °C. The integrated changes in enthalpy during precipitation of Fe are determined to be 24.7, 20.9 and 13.8 kJ/mol, for the three samples. Precipitation of Fe and Ag appears to be complete within the temperature of 750 °C. As evidenced from the DSC plots of all the samples, the sharp endothermic peak near 960 °C is due to the melting of the segregated silver crystals. Hence the thermodynamical assessment of the nanophase Ag–Fe alloys prepared in this work shows enthalpy states which are in agreement with the results reported based on DSC measurements carried out on ultra fine structures and theoretical calculations, though bulk Ag and Fe are immiscible and have a positive heat of mixing.

Table 1
Composition of Ag and Fe in Ag–Fe alloy samples as obtained from ICP-OES.

Sample	$AgNO_3$:$Fe(NO_3)_3$ molar ratio in precursor	Ag:Fe ratio in alloy by ICP-OES analysis
$Ag_{90}Fe_{10}$	90:10	96.6:03.4
$Ag_{75}Fe_{25}$	75:25	82.3:17.7
$Ag_{50}Fe_{50}$	50:50	53.7:46.3
$Ag_{25}Fe_{75}$	25:75	24.9:75.1

3.5. Microstructure

The FE-SEM images of Ag–Fe samples shown in Fig. 5 depicts agglomeration of particles resulting in different sizes and shapes. The micrograph of $Ag_{50}Fe_{50}$ sample shows particles of size 5–10 nm while $Ag_{75}Fe_{25}$ sample consists mostly of particles of irregular shapes whose sizes vary from 40 to 50 nm along with some very small particles of size of about 10 nm. Fig. 6 shows the HRTEM image of the as prepared $Ag_{50}Fe_{50}$ particles. These particles have agglomerated into dumbbell shaped ones whose widths are about 20–30 nm. Similar morphology has been reported by Elsukova et al. for the magnetron sputtered Ag–Fe nanoparticles [40]. The SAED pattern shown as inset in Fig. 6 is characteristic of polycrystalline particles. This could be due to the overlapping of the particles as seen in the micrograph since the XRD pattern of this sample shows single fcc phase.

3.6. Magnetic properties

The hysteresis loops of the Ag–Fe alloy samples obtained using VSM are shown in Fig. 7 and the magnetic measurements in Table 2. All the samples show soft ferromagnetic behavior with very low coercivity. The ferromagnetism in fcc Ag–Fe alloy could be due to the Fe atoms possessing a d band structure as explained by Stoner model [41]. Similar ferromagnetic behavior has been reported by Crespo et al. in the case of fcc Fe–Cu solid solution [42]. However there may be a small quantity of Fe particles within the superparamagnetic, single and multidomain ranges which would also contribute to the magnetization of these materials.

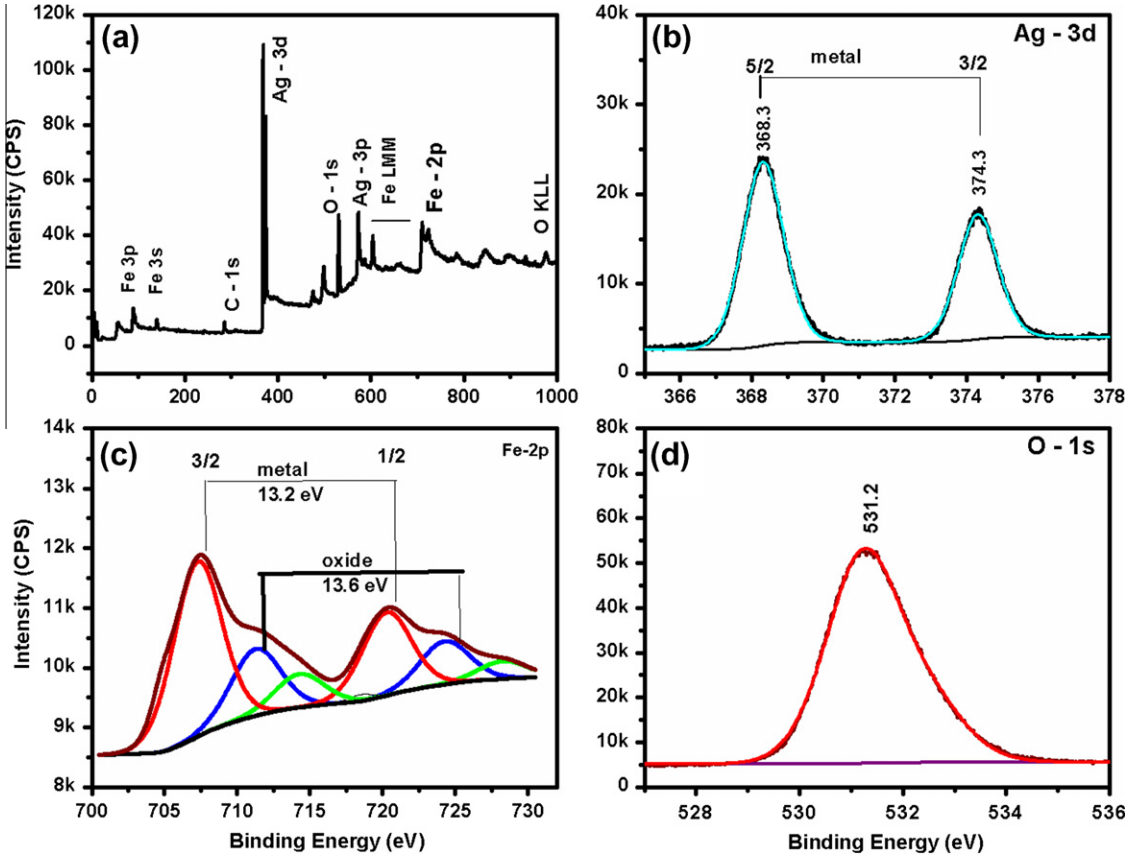

Fig. 3. XPS spectra of $Ag_{50}Fe_{50}$ sample. XPS spectra of $Ag_{50}Fe_{50}$ sample. (a) Wide scan XPS spectrum of $Ag_{50}Fe_{50}$. (b–d) High resolution spectra of Ag 3d, Fe 2p and oxygen 1 s regions.

The nature of interparticle magnetic interactions between the Fe atoms through nonmagnetic Ag spacer atoms, depends on the size of the Fe particles and the distance between them, which ultimately depend on its content. When the concentration of Fe atoms is less, the interparticle distance will be more, resulting in predominance of long range interactions and when the Fe content is more, strong short range interactions will take over. Hence in the case of $Ag_{90}Fe_{10}$ and $Ag_{75}Fe_{25}$ samples, the contribution will be largely due the RKKY (Ruderman–Kittel–Kasuya–Yosida) type interactions between the Fe ions through the conduction electrons of Ag [43]. $Ag_{90}Fe_{10}$ shows low magnetization which did not fully saturate upto 600 kA/m. As the Fe content is increased, it is found that the magnetization values increase more linearly at small applied fields as shown in the inset of Fig. 7. The as prepared samples which exhibit fcc structure show ferromagnetic nature. This magnetization should arise from the nanometric sized Fe particles which are embedded on the fcc matrix. However, the specific saturation magnetization (σ_s) values of the samples are not in direct proportion to the at.% of Fe in them as observed even by other studies [10]. A combined influence of surface effects and finite size effects govern the magnetic properties of granular alloys of magnetic and nonmagnetic metals and heterogeneous structures [44]. Surface effects play a significant role in the magnetic properties of nanoparticles since the ratio of surface spin to total spin increases with decrease in particle size. Therefore, the magnetization at the surface of the magnetic particles along the interfaces formed in granular alloys will not be uniform. In addition to the strong interchange interactions between particles and various other effects mentioned above, the magnetic character of alloys consisting of magnetic–nonmagnetic metals is also influenced by the magneto crystalline anisotropy and shape anisotropic effects [45]. The σ_s values and the coercivity of all the samples are shown in Table 2. The coercivity decreases with increase in Fe (upto 50% of Fe) and then shows an increase for the sample $Ag_{25}Fe_{75}$. The coercivity of the as prepared $Ag_{50}Fe_{50}$ sample is is observed to be 3.52 kA/m (44 Oe).

The magnetic characterization of the phases that resulted after annealing $Ag_{50}Fe_{50}$ at 300 °C, 400 °C and 500 °C was carried out and the results are shown in Fig. 8. With increase in annealing temperature, the magnetization also increases. The increase is not much pronounced up to an annealing temperature of 400 °C, the temperature up to which the material retains fcc phase. But after the heat treatment at 500 °C, the material shows a remarkable increase in its saturation magnetization value. This result is in correlation with the XRD analysis of the annealed samples. Up to 400 °C, though the magnetic Fe particles may slowly grow in size, as long as they remain in the fcc lattice along with the Ag atoms there is not much increase in saturation magnetization values due to the interfaces and the proximity effects. But as the sample is heat treated at 500 °C, the Fe particles leave the fcc lattice and begin to precipitate as can be speculated in the XRD pattern. This trend is also seen in the Curie transitions of the as prepared and the heat treated $Ag_{50}Fe_{50}$ samples. Fig. 9 shows the changes in the magnetic behavior of the samples with increase in temperature and their Curie transitions. The as prepared sample and the samples annealed at 300 and 400 °C do not show a sharp Curie transition but a gradual fall in specific magnetization with increase in temperature losing their magnetization approximately near the same temperature. These temperatures are 517, 553 and 567 °C for the three samples mentioned above. Liu et al. [21] have reported the Curie temperature of nanocrystalline Fe–Ag alloy to be around 570 °C which is in agreement with our observation. The behavior of the sample annealed at 500 °C is different from the other cases, in the sense that it shows a slight increase in magnetization with increase in tem-

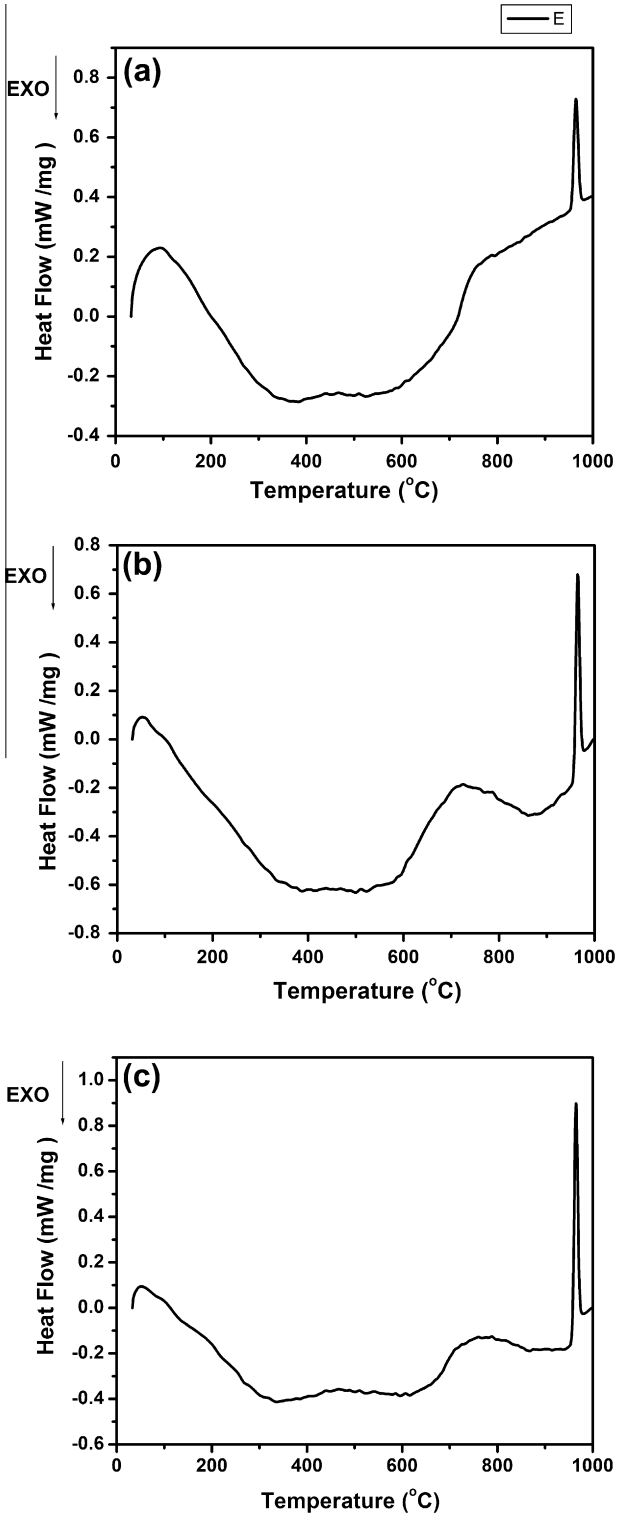

Fig. 4. DSC plots of (a) $Ag_{90}Fe_{10}$, (b) $Ag_{75}Fe_{25}$ and (c) $Ag_{50}Fe_{50}$ samples showing a complex broad exothermic peak from 150 °C to 750 °C indicating multiple processes which include disorder–order transition, grain growth and precipitation.

perature and a sharp fall indicating the Curie transition at 622 °C which is the same as that reported by Kataoka et al. for the Fe rich bcc Fe–Ag alloys [34]. This is the sample which shows precipitation of Fe as seen in the XRD patterns. The DSC thermographs also indicate segregation of metals above 400 °C.

Fig. 10a–c shows the room temperature Mössbauer spectra of the as prepared $Ag_{50}Fe_{50}$ sample and the same annealed at

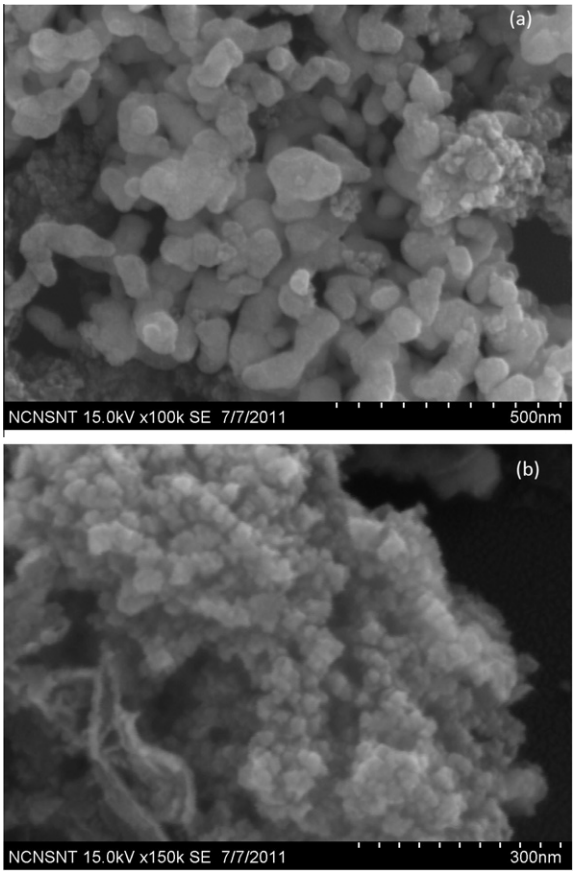

Fig. 5. FESEM images of the as prepared samples. FESEM images showing the morphology of (a) $Ag_{75}Fe_{25}$ and (b) $Ag_{50}Fe_{50}$.

300 °C and 500 °C. The spectrum of the as prepared sample shows a prominent doublet (QS = 0.70 mm/s, IS = 0.22 mm/s) arising from the intercalation of Fe atoms in fcc Ag lattice [2,46]. There is also a possibility of fine superparamagnetic Fe particles (IS = 0.05 mm/s, B_{hf} = 27 T) embedded in the Ag matrix. These values match with those reported by Alof et al. for the Ag–Fe alloy prepared by codeposition of the two metals in ultra high vacuum [47]. The sextet of low intensity superposed on the doublet is due to the small amount of Fe clusters which contribute to the ferromagnetic behavior of the material [48]. In the spectrum of the sample annealed at 300 °C for 1 h in vacuum, two ferromagnetic sextets corresponding to the bcc phase of Fe (IS = 0.01 mm/s, B_{hf} = 27 T) and iron oxide (IS = 0.40 mm/s, B_{hf} = 46 T) are detectable. Though the increase in intensity of the sextets indicates that the Fe clusters have grown in size, the phase segregation is not much pronounced at this temperature. The paramagnetic doublet (QS = 0.80 mm/s, IS = 0.20 mm/s) which signifies the presence of Fe atoms in the fcc matrix is still speculated in the fitted spectrum with less intensity. These results suggest that the nearest neighbor contribution has not undergone any remarkable change on annealing 300 °C. In the case of the sample annealed at 500 °C, the sextet corresponding to bcc Fe (IS = 0.01 mm/s, B_{hf} = 29 T) shows further increase in its intensity indicating phase segregation. The intensity of sextet that pertains to iron oxide (IS = 0.40 mm/s, B_{hf} = 46 T) has also increased with a decrease in that of the doublet (QS = 0.60 mm/s, IS = 0.20 mm/s) signifying that Fe atoms incorporated in the fcc lattice begin to precipitate [34]. Hence the Mossbauer study of our samples was used to confirm the conclusions drawn on phase transformation and changes in magnetic properties with temperature.

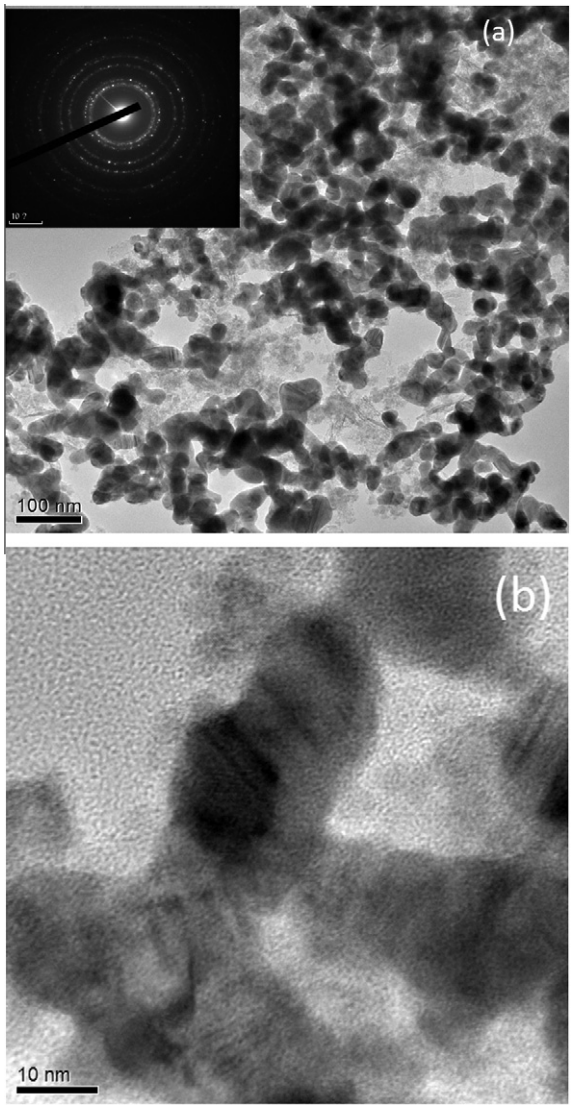

Fig. 6. HRTEM micrograph of Ag_{50} Fe_{50} sample. The inset figures show the SAED pattern of the sample.

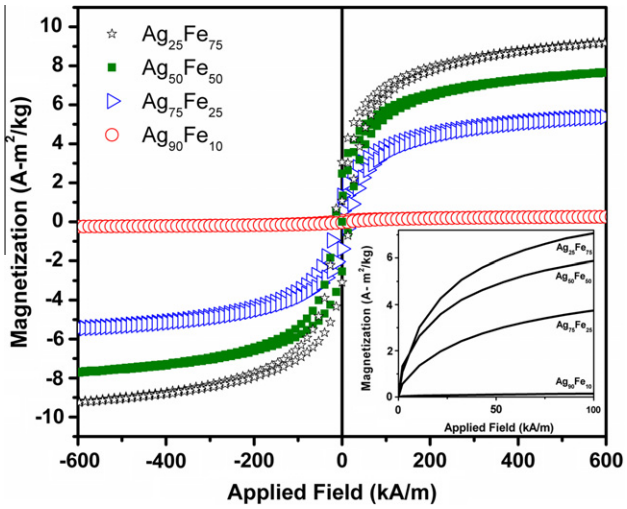

Fig. 7. Magnetization behavior of as synthesized samples. Magnetic hysteresis curves of Ag_{90} Fe_{10}, $Ag_{75}Fe_{25}$, $Ag_{50}Fe_{50}$ and $Ag_{25}Fe_{75}$ samples taken at room temperature. The inset shows the samples attaining saturation magnetization at low applied fields.

Table 2
Magnetic data of the as prepared and the annealed Ag–Fe alloy samples.

Sample	Fe content (at.%)	Saturation magnetization (σ_s) (A-m^2/kg)	Coercivity (H_c) (kA/m)	Remanence (M_R) (A-m^2/kg)
$Ag_{90}Fe_{10}$ (as prepared)	03.40	00.25	06.12	00.02
$Ag_{75}Fe_{25}$ (as prepared)	17.70	05.39	04.08	00.42
$Ag_{50}Fe_{50}$ (as prepared)	46.30	07.74	03.52	00.76
$Ag_{50}Fe_{50}$ (T_A = 300 °C)		08.10	04.33	00.88
$Ag_{50}Fe_{50}$ (T_A = 400 °C)		08.76	04.37	00.91
$Ag_{50}Fe_{50}$ (T_A = 500 °C)		20.52	07.40	02.21
$Ag_{25}Fe_{75}$ (as prepared)	75.10	009.31	07.55	03.55

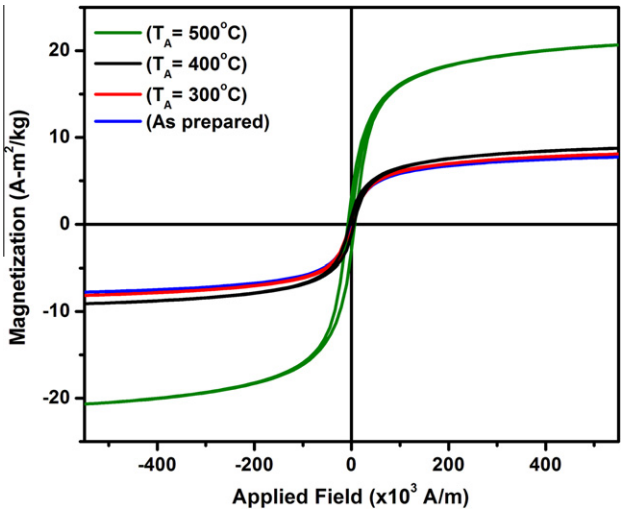

Fig. 8. Magnetization behavior of annealed samples. Effect of annealing on the magnetization behavior of $Ag_{50}Fe_{50}$ sample annealed at 300 °C, 400 °C and 500 °C for 1 h each.

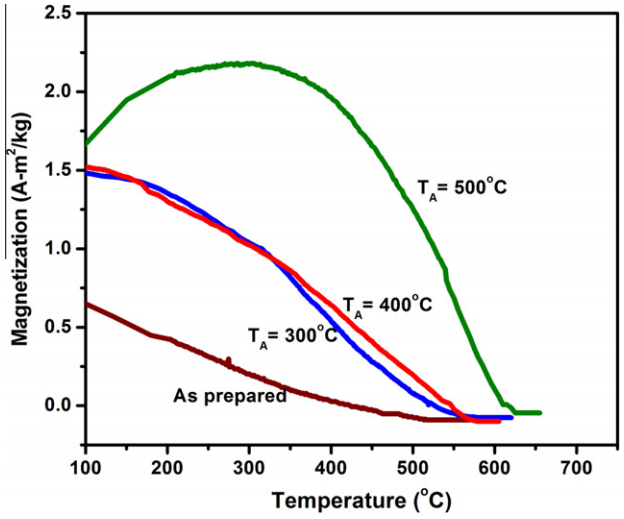

Fig. 9. Magnetic behavior of the as prepared and annealed $Ag_{50}Fe_{50}$ samples. Sample annealed at 500 °C shows Curie transition at 622 °C.

4. Conclusions

This work proves that alloy formation of nano-phase Ag–Fe is possible even in the as prepared samples synthesized by sodium borohydride reduction. This is a fairly simple method which can be carried out at normal conditions for large scale production of

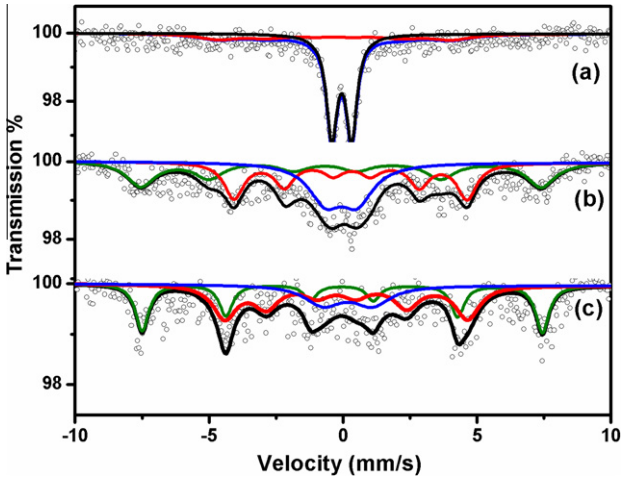

Fig. 10. Mössbauer spectra of $Ag_{50}Fe_{50}$ sample (a) as prepared (b) annealed at 300 °C and (c) annealed at 500 °C. (Experimental data (circles), doublet (blue line), Fe sextet (red line), iron oxide (green line) and over all fitted spectrum (black line).) (For interpretation of the references to color in this figure legend, the reader is referred to the web version of this article.)

Ag–Fe alloy, which can be a suitable material for GMR applications. The composition of the alloy is controllable by modifying the precursor ratio. The alloy thus obtained in different compositions is metastable. The materials retain fcc structure upto an annealing temperature of 400 °C beyond which the transformation of fcc phase into fcc and bcc phases is effected due to precipitation of the magnetic component. The DSC studies and the thermodynamical calculations made there from also reveal the same trend. This is further confirmed by the magnetic measurements according to which the as prepared sample shows almost the same saturation magnetization and Curie temperature even after annealing up to 400 °C for 1 h in vacuum. There is a significant change in magnetization values and in the trend in Curie transition for the sample annealed at 500 °C. From the magnetic behavior and the Mössbauer studies of the samples, it is inferred that in the as prepared materials along with the Fe atoms in Ag lattice, there may be ultra fine Fe particles present in the fcc Ag matrix and precipitation of Fe occurs on annealing. Hence all these results are in support of the fact the Ag–Fe alloy synthesized by chemical reduction method is metastable and it undergoes significant changes in structure and magnetic properties on heating beyond 400 °C.

Acknowledgements

The authors wish to thank Dr. D. Prabhu and Dr. N. Ponpandian for the fruitful discussions with them and Mr. B. Sounderarajan for his support in carrying out the magnetic measurements. We acknowledge the FESEM facilities provided by the National Centre for Nanoscience and Nanotechnology, University of Madras and the ICP-OES facility provided by DST and SAIF, IIT Madras.

Appendix A. Supplementary material

Supplementary data associated with this article can be found, in the online version, at http://dx.doi.org/10.1016/j.jallcom.2012.12.161.

References

[1] L.J. Swartzendruber, Bull. Alloy Phase Diagram 5 (1984) 560–564.
[2] S. Xiao, W. Hua, W. Luo, Y. Wu, X. Li, H. Deng, Eur. Phys. J. B 54 (2006) 479–484.
[3] M.K. Roy, P.M.G. Nambissan, H.C. Verma, J. Alloys Compd. 345 (2002) 183–188.
[4] G. Xiao, J.Q. Wang, J. Appl. Phys. 75 (10) (1994) 6604–6606.
[5] Y. Nakamura, K. Sumiyama, N. Kataoka, Hyperfine Interact. 28 (1986) 1029–1032.
[6] J.M. Soares, J.H. de Araujo, F.A.O. Cabral, T. Dumelow, F.L.A. Machado, A.E.P. de Araujo, Appl. Phys. Lett. 80 (14) (2002) 2532–2534.
[7] N. Thangaraj, C. Echer, K.M. Krishnan, R.F.C. Farrow, R.F. Marks, S.S.P. Parkin, J. Appl. Phys. 79 (1994) 6900–6902.
[8] E. Ma, J.H. He, P.J. Schilling, Phys. Rev. B 55 (9) (1997) 5542–5545.
[9] R.L. Zong, S.P. Wen, F. Zeng, Y. Gao, C. Song, B. He, F. Pan, Appl. Surf. Sci. 253 (2007) 2993–2998.
[10] J.M. Soares, J.H. de Aroujo, F.O.C. de Assis, T. Dunelow, M.M.X. Junior, J.M. Sasaki, Mat. Res. 8 (2005) 347–350.
[11] P. Crespo, A. Hernando, R. Yuvari, R. Yuvari, O. Drbohlav, A.G. Escorial, J.M. Barandiaran, I. Orue, Phys. Rev. B. 48 (1993) 7134–7139.
[12] S. Arana, N. Arana, F.J. Gracia, E. Castano, Sensors Actuat A 123–124 (2005) 116–121.
[13] G. Mihajlović, K.D. Schreiber, Y. Liu, J.E. Pearson, S.D. Bader, A.K. Petford-Long, A. Hoffmann, Appl. Phys. Lett. 97 (2010) 112502.
[14] M.L. Yan, H. Zeng, N. Powers, D.J. Sellmyer, J. Appl. Phys. 91 (2002) 8471–8473.
[15] Y. Sun, B. Mayers, Y. Xia, Nano Lett. 3 (2003) 675–679.
[16] A. Roy, V. Srinivas, S. Ram, J.A. De Toro, U. Mizutani, Phys. Rev. B. 71 (2005) 184443-1–184443-10.
[17] K. Santhi, E. Thirumal, S.N. Karthick, H.J. Kim, M. Nidhin, V. Narayanan, A. Stephen, J. Nanopart. Res. 14 (868) (2012) 1–12.
[18] L. Dimesso, G. Miehe, H. Fuess, H. Hahn, J. Magn. Magn. Mater. 191 (1999) 162–168.
[19] J. Alanso et al., Nanotechnology 23 (2012) 025705. 1–10.
[20] J.Q. Wang, G. Xaio, Phys. Rev. B 49 (1994) 3982. 1–17.
[21] S. Liu et al., J. Magn. Magn. Mat. 233 (2001) 195–204.
[22] N. Kataoka, K. Sumiyama, Y. Nakamura, J. Phys. F: Met. Phys. 15 (1985) 1405–1411.
[23] C.-Y. Tung, H.-M. Lin, J.M. Gu, P.-Y. Lee, Nanostruct. Mater. 9 (1997) 117–120.
[24] V.V. Hiep, N. Chau, D.M. Hong, N.H. Luong, J. Magn. Magn. Mater. 310 (2007) 2524–2526.
[25] J.H. Du, Q. Li, L.C. Wang, H. Sang, S.Y. Zhang, Y.W. Du, D. Feng, J. Phys.: Condens. Matter 7 (1995) 9425–9432.
[26] M. Störmer, H.-U. Krebs, J. Appl. Phys. 78 (1995) 7080–7087.
[27] X. Qingmei, Z. Yao, J. Liu, R. Hai, H.Y. Oderji, H. Ding, Thin Solid Films 519 (2011) 7116–7119.
[28] P.R. Sajanlal, T. Pradeep, J. Phys. Chem. 114 (2010) 16051–16059.
[29] J.F. Moulder, W.F. Stickle, P.E. Sobel, K.D. Bomben, Hand book of X-ray photoelectron spectroscopy, in: Jill Chastain, Roger C. King, Jr.,(Eds): ULVAC-PHI, Inc., Japan, Physical Electronics USA Inc., USA, 1993.
[30] A. Lebugle, U. Axelson, R. Nyholm, N. Martensson, Phys. Scr. 23 (1981) 825–827.
[31] K. Asami, J. Electron Spectrosc. Relat. Phenom. 9 (1976) 469–478.
[32] N.S. McIntyre, D.G. Zetaruk, Anal. Chem. 49 (1977) 1521–1529.
[33] C.D. Wagner, D.A. Zatco, R.H. Raymond, Anal. Chem. 52 (1980) 1445–1451.
[34] N. Kataoka, K. Sumiyama, Y. Nakamura, Acta Metall. 37 (1989) 1135–1142.
[35] J.H. He, H.W. Sheng, E. Ma, Appl. Phys. Lett. 78 (2001) 1343–1345.
[36] J. Eckert, J.C. Holzer, C.E. Krill III, W.L. Johnson, J. Appl. Phys. 6 (73) (1993) 2794–2802.
[37] B.N. Mondal, A. Basumallick, P.P. Chattopadhyay, J. Magn. Magn. Mater. 309 (2007) 290–294.
[38] A. Stephen, F. Rossi, L. Nasi, C. Ferrari, N. Ponpandian, M.V. Ananth, V. Ravichandran, J. Appl. Phys. 103 (2008) 53511-1–53511-8.
[39] M. Huang, J. Appl. Phys. 97 (2005) 64906-1–64906-6.
[40] A. Elsukova, Z. Li, C. Moller, M. Spasova, M. Acet, M. Farle, M. Kawasaki, P. Ercius, T. Duden, Phys. Status Solidi A 208 (2011) 2437–2442.
[41] P.M. Marcus, V.L. Moruzzi, Phys. Rev. B 38 (1998) 6949–6953.
[42] P. Crespo, A. Hernando, R. Yavari, O. Drbohlav, E.A. Garcia, J.M. Barandiaran, I. Orue, Phys. Rev. B 48 (1993) 7134–7139.
[43] A.S. Nicola, Magnetic Materials – Fundamentals and Applications, second ed., Cambridge University Press, New York, 2010.
[44] B. Xavier, L. Amilcar, J. Phys. D. Appl. Phys. 35 (2002) R15–R42.
[45] E.C. Stoner, E.P. Wohlfarth, Philos. Trans. R. Soc. Lond. A 240 (1948) 599–642.
[46] S.A. Makhlouf, K. Sumiyama, H. Onodera, K. Wakoh, K. Suzuki, Nucl. Instrum. Methods Phys. Res. B 76 (1993) 197–198.
[47] C. Alof, B. Stahl, M. Ghafari, H. Hahn, J. Appl. Phys. 88 (2000) 4212–4215.
[48] J. Kuyama, H. Inui, S. Imaoka, S. Nasu, N. Keiichi, P.H. Ishhara, J. Shingu, J. Appl. Phys. 30 (1991) L854–L856.